International Journal of Heat and Fluid Flow 30 (2009) 1037–1043

Contents lists available at ScienceDirect

International Journal of Heat and Fluid Flow

journal homepage: www.elsevier.com/locate/ijhff

Numerical simulation of the turbulent wake behind a normal flat plate

Vagesh D. Narasimhamurthy *, Helge I. Andersson

Fluids Engineering Division, Department of Energy and Process Engineering, Norwegian University of Science and Technology (NTNU), 7491 Trondheim, Norway

ARTICLE INFO

Article history:
Received 23 July 2008
Received in revised form 13 August 2009
Accepted 5 September 2009
Available online 12 October 2009

Keywords:
Uniform plate
Parallel-sided plate
DNS
Turbulence
Wake flow
Normal flat plate

ABSTRACT

The three-dimensional wake flow behind a flat plate placed normal to the free stream has been investigated by means of direct numerical simulations. The Reynolds number *Re* based on the homogeneous inflow velocity and the uniform width *d* of the plate was 750. Coherent vortices were alternately shed from the sides of the plate with a frequency corresponding to a Strouhal number 0.168. The wake was distinctly turbulent downstream of the plate whereas the mean recirculation bubble extended 1.96*d* downstream. A steady 2D mean flow and the accompanying Reynolds stresses were obtained by averaging in time and along the span of the plate. These Reynolds-averaged statistics exhibited the same qualitative features as corresponding data from cylinder wakes.

1. Introduction

Vortex shedding from bluff bodies, and particularly from two-dimensional bluff bodies, is one of the most studied research topics in fluid mechanics. Among such two-dimensional bluff bodies, the normal flat plate, i.e. a uniform flat plate placed normal to the free-stream, is the simplest configuration that can yield complex wake flow phenomena. Unlike the case of circular or elliptic cylinders, the flow past a normal flat plate is characterized by fixed separation points and the separated near-wake is known to remain symmetrical and steady in the Reynolds number range $Re = 5-20$ (Dennis et al., 1993). Recently, Saha (2007) reported that the separated near-wake of a normal flat plate undergoes a Hopf bifurcation, i.e. transition from a steady state to an unsteady state, at a Reynolds number that lies in between 30 and 35. It is also known from the existing literature that a second transition, which renders the flow three-dimensional (and eventually turbulent) occurs already at $Re = 105-110$ (Thompson et al., 2006).

If we now focus our attention on turbulent wakes, it is surprising to see that almost all the turbulent flow cases are either studied by experiments or by means of two-dimensional (2D) simulations (see Table 1). The only exception is the Direct Numerical Simulation (DNS) carried out by Najjar and Vanka (1995a) where they provided some data of the mean integral parameters such as the drag coefficient and the base pressure coefficient. Their objective, however, was limited to study and compare the drag characteristics obtained from a three-dimensional simulation with those obtained from an equally resolved 2D simulation. Kiya and Matsumura (1988), Leder (1991) and Mazharoglu and Hacışevki (1999) presented phase-averaged rather than time-averaged flow statistics. Kiya and Matsumura (1988) used hot-wire anemometry and measured all three velocity components 8*d* downstream of the plate while Leder (1991) employed non-intrusive laser-Doppler anemometry to provide data in the immediate vicinity of the plate. The Reynolds number in these two investigations was roughly the same, see Table 1. Both introduced a triple-decomposition of the velocity field to distinguish between the time–mean value $\overline{U}$, the quasi-periodic coherent shedding $\tilde{u}$ and the incoherent random turbulence u'. Their phase-averaged data shed light on the vortex dynamics in the flat plate wake. Even though these experimental studies documented the turbulence statistical quantities, they were nevertheless carried out at high Reynolds numbers. Moreover, experimental methods cannot capture the complete three-dimensional data. In contrast, the 2D numerical simulations are known to overpredict the drag and base suction coefficients and underpredict the recirculation length (Najjar and Vanka, 1995a; Mittal and Balachandar, 1995). An in-depth and comprehensive study of the turbulent wake behind a normal flat plate is therefore awaited. DNS as a tool is the natural choice in the present investigation, as it gives complete access to the instantaneous three-dimensional flow field. In addition to frequency analysis and vortical structure information, a detailed analysis of Reynolds-averaged statistical quantities will be presented.

* Corresponding author. Tel.: +47 73593563; fax: +47 73593491.
E-mail address: vagesh@ntnu.no (V.D. Narasimhamurthy).

0142-727X/$ - see front matter © 2009 Elsevier Inc. All rights reserved.
doi:10.1016/j.ijheatfluidflow.2009.09.002

Table 1
Various studies on flow past normal flat plates.

Case	*Re*	Flow regime	Method
Present study	750	Turbulence	3D-numerical
Fage and Johansen (1927)	1.5×10^5	Turbulence	Experiments
Mazharoglu and Hacışevki (1999)	3.3×10^4	Turbulence	Experiments
Leder (1991)	2.8×10^4	Turbulence	Experiments
Kiya and Matsumura (1988)	2.3×10^4	Turbulence	Experiments
Wu et al. (2005)	1.8×10^3–2.7×10^4	Turbulence	Experiments
Najjar and Vanka (1995b)	100–1000	Turbulence	2D-numerical
Tamaddon-Jahromi et al. (1994)	126–500	Turbulence	2D-numerical
Najjar and Vanka (1995a)	1000	Turbulence	3D-numerical
Najjar and Balachandar (1998)	250	Transition	3D-numerical
Julien et al. (2003)	200–220	Transition	Experiments
Julien et al. (2004)	220	Transition	2D-numerical
Saha (2007)	30–175	Laminar	2D-numerical
Dennis et al. (1993)	5–20	Laminar	Experiments

2. Flow configuration and numerical method

We considered the flow past a normal flat plate with the view to explore the vortex shedding at moderately high Reynolds numbers, i.e. sufficiently high to make even the near-wake turbulent. The Reynolds number *Re* based on the uniform inflow velocity U_o and the width of the plate d was equal to 750. The size of the computational domain in the streamwise (X), spanwise (Y) and the cross-stream (Z) directions were $L_x = 25d$, $L_y = 6d$, and $L_z = 16d$, respectively, as shown in Fig. 1. All spatial dimensions are normalized by d and all velocities are scaled with the uniform inflow velocity U_o. The thickness of the plate was very small and equal to $0.02d$.

The Navier–Stokes equations in *incompressible* form were solved in 3D space and time using a *parallel* finite-volume code called MGLET (Manhart, 2004; Narasimhamurthy et al., 2008). The code uses staggered Cartesian grid arrangements. Discretization of the spatial derivatives was achieved by means of a 2nd-order central-differencing scheme. The time marching was carried out using a 3rd-order explicit Runge–Kutta scheme for the momentum equations in combination with an iterative SIP (Strongly Implicit Procedure) solver for the Poisson equation. The number of grid points in each coordinate direction ($N_x \times N_y \times N_z$) is shown in Table 2 and compared with the previous DNS studies on normal flat plates (Najjar and Vanka, 1995a; Najjar and Balachandar, 1998). The time step was chosen as $\Delta t = 0.001d/U_o$ and the number of Poisson iterations per time step was limited to 60. The computations were performed on an *IBM P575+* parallel computer.

In order to justify that the present simulation is a fully resolved DNS, i.e. that all essential turbulent scales are captured, the grid size can be compared with Kolmogorov's microscale $\eta = (\nu^3/\varepsilon)^{1/4}$. Here, ε is the time–mean dissipation rate of fluctuating kinetic energy defined as

Table 2
Geometrical and grid parameters.

Case	N_x	N_y	N_z	L_x	L_y	L_z	*Re*
Present DNS	512	60	384	25	6	16	750
Najjar and Vanka (1995a)	256	32	256	28	2π	16	1000
Najjar and Balachandar (1998)	192	48	128	25	2π	16	250

$$\varepsilon = \nu\left(\overline{\frac{\partial u_i}{\partial X_j}\frac{\partial u_i}{\partial X_j}} + \overline{\frac{\partial u_i}{\partial X_j}\frac{\partial u_j}{\partial X_i}}\right) \approx \nu\left(\overline{\frac{\partial u_i}{\partial X_j}\frac{\partial u_i}{\partial X_j}}\right) \tag{1}$$

where u_i is the fluctuating part of the instantaneous velocity component which comprises both the unsteady fluctuations and the turbulent fluctuations. The contribution from the second term in the above definition of the total dissipation rate ε is negligible (Bradshaw and Perot, 1993) and hence neglected in the present analysis. The grid size relative to the Kolmogorov microscale at five different downstream positions are given in Table 3 and compared with corresponding data for the plane wake DNS by Moser et al. (1998) and the trailing-edge wake DNS of Yao et al. (2001). The data in Table 3 shows that the grid size in the present study is of the same order of magnitude as the Kolmogorov length scale. The present grid resolution compares favorably with that used in other wake flow simulations.

A uniform velocity profile $U_o = 1$ was prescribed at the inlet without any free-stream perturbations and a Neumann boundary condition was used for the pressure. A free-slip boundary condition was applied on both the top and the bottom wall and a periodic boundary condition was used for the side walls (cf. Fig. 1). At the outlet, a Neumann boundary condition was used for velocities and the pressure was set to zero. A *direct forcing* Immersed Boundary Method (Peller et al., 2006; Narasimhamurthy et al., 2008) was used to transform the no-slip condition at the plate surface into internal boundary conditions at the nodes of the Cartesian grid.

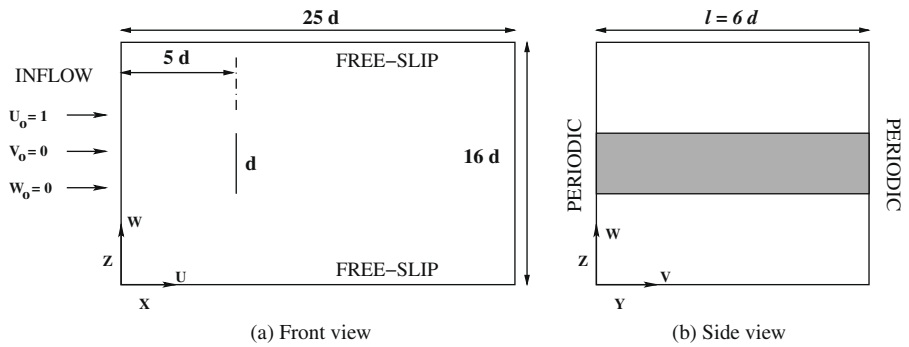

(a) Front view (b) Side view

Fig. 1. Computational domain (not to scale).

Table 3
Grid resolution at various X/d positions measured from the axis of the plate.

X/d		1	3	5	8	12
Present DNS	$\Delta X/\eta$	3.48	2.69	2.19	1.87	1.65
	$\Delta Y/\eta$	7.98	6.15	4.97	4.22	3.71
	$\Delta Z/\eta$	1.99	1.54	1.24	1.05	0.92
Yao et al. (2001)	$\Delta X/\eta$	6.88	5.07	3.42	2.76	2.44
Moser et al. (1998)	$\Delta X/\eta$			≈15		

The internal boundary condition value had to be determined by interpolation. In the present DNS we used least-squares interpolation of 3rd-order accuracy. The detailed derivation, validation and implementation of this technique in the code MGLET were explained in Peller et al. (2006).

3. Results and discussion

3.1. Wake pattern and frequency analysis

In order to identify the topology of the vortex cores correctly the λ_2-definition by Jeong and Hussain (1995) was used. λ_2 corresponds to the second largest eigenvalue of the symmetric tensor $S_{ij}S_{ij} + \Omega_{ij}\Omega_{ij}$, where S_{ij} and Ω_{ij} are, respectively, the symmetric and antisymmetric parts of the velocity gradient tensor. Iso-surfaces of negative λ_2 at time $t = 120d/U_o$ is shown in Fig. 2a. Note that the shear layer extends downstream of the plate by about two plate widths before rolling-up. The top view or the spanwise view of the same flow field is shown in Fig. 2b and the corresponding iso-pressure $\left(P/\rho U_o^2\right)$ contours are plotted in Fig. 2c. The spanwise vortex filaments are shed parallel to the axis of the plate but experience vortex stretching and twisting. The vortices appear to be highly irregular in the near wake and eventually break up into incoherent motion further downstream.

The time evolution of the instantaneous velocity components U, V, W and the instantaneous pressure, P, were sampled along two lines parallel to the axis of the plate and located $3d$ and $6d$ downstream the axis in X-direction, respectively. Both lines were offset by $0.5d$ in Z-direction. It would be inappropriate to present all the data here due to space constraints. Therefore, only the time trace of the cross-stream velocity W sampled at $3d$ is shown in Fig. 3a. The total sampling time was equal to $120d/U_o$, which covers about 20 vortex shedding cycles. The present sampling length was found to be long enough for the results to converge to a statistically stationary state. The spatio-temporal variations of W in Fig. 3a clearly demonstrate the parallel-shedding feature of the wake. To enable quantitative comparisons the frequency spectra were obtained from the Fast Fourier Transform (FFT) of the cross-stream velocity (W) time traces. A sample spectrum is shown in Fig. 3b, which is

(a) – λ_2 contours (streamwise view)

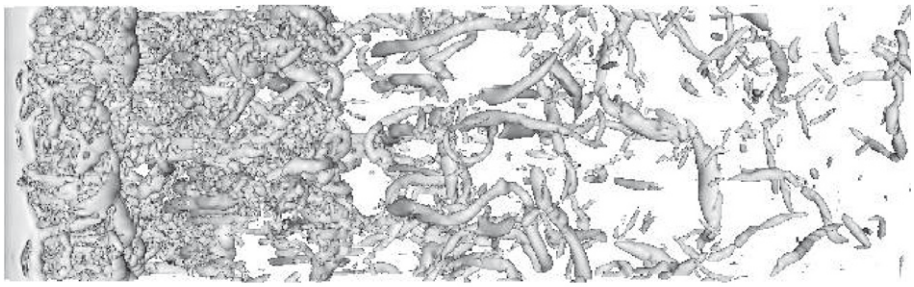

(b) – λ_2 contours (spanwise view)

(c) Iso-pressure ($P/\rho U_o^2 = -0.1$) contours (spanwise view)

Fig. 2. Three-dimensional vortical structures at the same instant in time, $t = 120\ d/U_o$. The plate is located on the left side and the flow direction is from left to right.

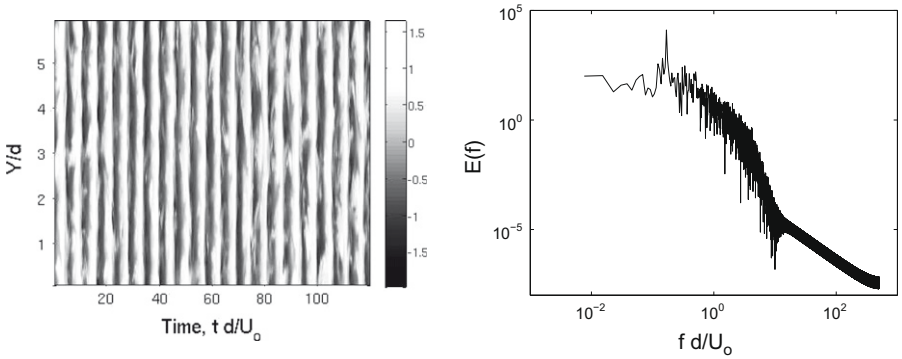

Fig. 3. (a) Time traces of the cross-stream velocity (W) component along the entire span. The sampling line is at $X/d = 3$ (measured from the axis of the plate) and $Z/d = 7.5$. (b) Power spectrum indicating the dominant frequency at $fd/U_o = 0.168$.

taken at the mid-span of the plate and is provided in a double-logarithmic plot. The primary shedding frequency corresponds to the most energetic frequency which is found at $fd/U_o = 0.168$. In Table 4 the Strouhal number (fd/U_o) from the present DNS is compared with earlier studies on normal flat plates. It can be observed that the present value is in close agreement with the previous low-Re studies carried out at $Re \leqslant 250$ (Saha, 2007; Najjar and Balachandar, 1998). In contrast, the Strouhal number from Najjar and Vanka (1995a) at $Re = 1000$ is in close agreement with the higher Reynolds number case (Kiya and Matsumura, 1988). The exceptionally low Strouhal number reported by Najjar and Vanka (1995a) is perhaps due to the shear-layer instabilities, which are known to occur at higher Reynolds numbers. Another possible reason could be the lower grid resolution used in their DNS study (cf. Table 2).

Table 4
Strouhal number (St), recirculation length (L_w) and mean drag coefficient ($\overline{C}_D$) data from various studies. Here $\overline{C}_D = 2F/(\rho U_o^2 A)$, where F is the drag force and A is the surface area of the plate.

Case	$St = fd/U_o$	L_w/d	$\overline{C}_D$	Re
Present study	0.168	1.96	2.31	750
Saha (2007)	0.1665		2.54	150
Saha (2007)	0.1640		2.56	175
Najjar and Balachandar (1998)	0.1613	2.35	2.36	250
Najjar and Vanka (1995a)	≈0.143	2.55	2.26	1000
Kiya and Matsumura (1988)	0.146			2.3×10^4
Fage and Johansen (1927)			2.13	1.5×10^5

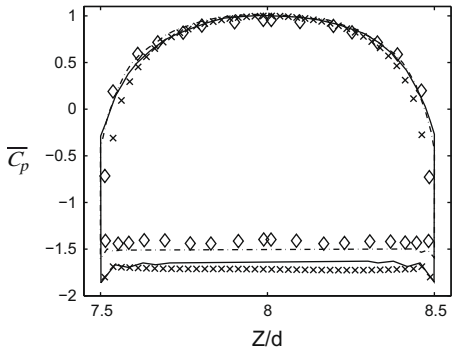

Fig. 4. Distribution of the mean pressure coefficient, $\overline{C}_p$, on the surface of the plate from the present DNS: $\times, Re = 750$; compared with the experimental data of Fage and Johansen (1927): $\diamond, Re = 1.5 \times 10^5$; and the DNS results of Najjar and Vanka (1995a): $-.-, Re = 1000$; Najjar and Balachandar (1998): $-, Re = 250$.

3.2. Mean pressure coefficient and recirculation length

Time-averaged statistical quantities were evaluated by sampling for $120d/U_o$ time units. One sample is taken every tenth time step for averaging. The three-dimensional data is then averaged in the spanwise Y-direction, i.e. in the direction of homogeneity. The mean pressure coefficient is defined as, $\overline{C}_p = 2(\overline{P} - P_\infty)/\left(\rho U_o^2\right)$, where the reference pressure P_∞ is taken from the pressure at the inflow and the overbar signifies averaging in time and spanwise direction. The distribution of $\overline{C}_p$ on the surface of the plate from the present DNS is compared against the earlier experimental (Fage and Johansen, 1927) and numerical (Najjar and Vanka, 1995a; Najjar and Balachandar, 1998) data in Fig. 4. The pressure on the upstream surface of the plate compares well with the previous data. The constancy of the pressure in the base region is well captured in the present DNS. However, the pressure in the base region is relatively lower compared to the prediction of Najjar and Vanka (1995a). This could again be a pure Reynolds number effect as discussed in the previous section or perhaps due to the modest grid resolution used in Najjar and Vanka (1995a).

The coupling suggested by Bearman (1965, 1967) and others between the base pressure and the vortex formation process can be explored in the present study. If we compare the base pressure values in Fig. 4 with the corresponding Strouhal numbers in Table 4, it is apparent that the reduction in base pressure causes an increase in St, i.e. gives rise to a stronger vortex shedding. A very strong and periodic vortex shedding eventually produces shorter recirculation lengths. It can be observed from Table 4 that the recirculation length L_w decreases with an increase in St and vice versa. Thereby, the coupling between the wake recirculation length L_w and the base pressure is explained. In the present context the recirculation length L_w, i.e. the length of the mean recirculation bubble (see Fig. 5a), is defined as the streamwise distance from the axis of the plate to the position where the mean streamwise velocity $\overline{U}$ changes sign from negative to positive (see Fig. 5b).

3.3. Reynolds-averaged statistics

It is important to quantify the growth and decay of different properties of the fluctuating motion, especially in the near wake region where the similarity laws are not valid. Therefore in the present section Reynolds-averaged statistical quantities at some sections downstream of the plate will be presented and the underlying physics will be discussed. It can be observed from Fig. 5b that

the mean cross-stream velocity $\overline{W}$ is zero along the wake centerline. Note that the wake centerline is subjected to an equally weighted influence of both the alternating vortices shed from either side of the plate. The observation that $\overline{W} \approx 0$ along the wake centerline reconfirms that the present statistics are fully converged to a stationary state. The variation of the mean streamwise velocity $\overline{U}$ in the near wake at five different positions downstream of the plate is shown in Fig. 6a. The negative velocity at the location $X/d = 1$ stems from the recirculation zone. Along the wake centerline at $X/d = 2$, $\overline{U}$ is nearly zero since this position is very close to the free stagnation point. The mean cross-stream velocity ($\overline{W}$) profiles are shown in Fig. 6b. The anti-symmetric variation of $\overline{W}$ is consistent with the symmetry of $\overline{U}$.

It is noteworthy that the largest cross-flow velocity occurs aside of the free stagnation point, as one could expect from the streamline pattern in Fig. 5a. The largest cross-flow velocity $\overline{W}$ is close to 0.2 U_o, whereas the largest velocity defect is about 0.45 U_o according to Fig. 5b. The latter corresponds well with the maximum velocity defect 0.4 U_o found by Kiya and Matsumura (1988) at $X/d = 8$. Outside of the recirculation bubble, the cross-flow $\overline{W}$ is mostly directed away from the symmetry line while the cross-flow within and downstream of the bubble, i.e. for $X/d \geqslant 1$, is towards the centerline.

The Reynolds-averaged statistics were obtained by sampling over a time interval 120 d/U_o and thereafter averaging in the statistically homogeneous Y-direction. This averaging leaves two-dimensional fields of the mean velocity components $\overline{U}(X,Z)$ and $\overline{W}(X,Z)$ and similarly for the Reynolds stress components and the energy dissipation rate. Two of the off-diagonal components of the Reynolds-stress tensor, i.e. $\overline{uv}$ and $\overline{vw}$, are zero due to the symmetries of the present flow. Reynolds stresses $\overline{u^2}, \overline{v^2}, \overline{w^2}$ and $\overline{uw}$ are plotted in Fig. 7a, b, c and d, respectively. Note that due to the Reynolds-averaging, the stress components have contributions from both the unsteady fluctuations and the turbulent fluctuations. Perrin et al. (2006) recently presented PIV-data acquired from the near-wake of a circular cylinder at high Reynolds numbers. The contour plots of the time-averaged PIV data of Perrin et al. (2006) show an almost complete qualitative agreement with the present DNS data, in spite of the difference in Reynolds number.

The present observation that maximum value of $\overline{w^2}$ is about twice as high as the highest level of $\overline{u^2}$ is in accordance with the DNS data of a transitional cylinder near-wake by Persillon and Braza (1998) and the fully turbulent near-wake PIV data by Perrin et al. (2006). Kiya and Matsumura (1988) presented measurements of the coherent and incoherent velocity fluctuations behind a flat plate. At $X/d = 8$, the two parts contributed nearly equally to $\overline{w^2}$, which was roughly twice of $\overline{u^2}$. The streamwise fluctuations, on the other hand, stemmed mostly from the incoherent (i.e. turbulent) motions. From their phase-averaged field, Perrin et al. (2006) observed that the high values of $\overline{\tilde{w}^2}$ were associated with the centers of the shed vortices. They also examined some different terms for the kinetic energy production and consistently found that the turbulent energy was produced in the shear layers just downstream of where the flow separates from the bluff body. It was therefore suggested that turbulent energy is transported from the shear layers to the centre of the wake where the highest energy levels are observed. We certainly support this point of view. However, the turbulence production in the shear layers will predominately generate streamwise velocity fluctuations due to the

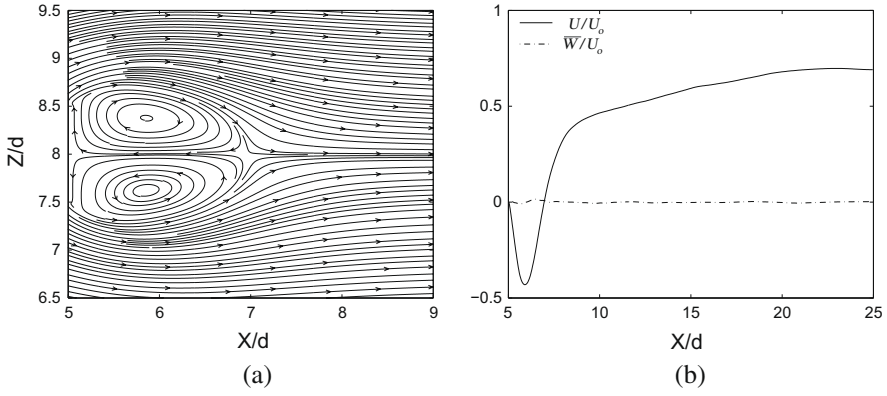

Fig. 5. (a) Streamlines showing the mean recirculation bubble. (b) Time–mean velocity profiles along the wake centerline.

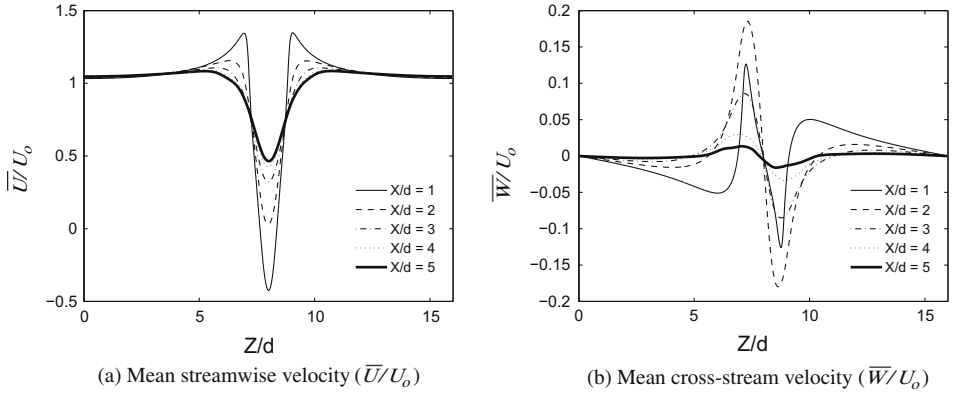

(a) Mean streamwise velocity ($\overline{U}/U_o$) (b) Mean cross-stream velocity ($\overline{W}/U_o$)

Fig. 6. Mean velocity profiles at fixed X/d positions (measured from the axis of the plate).

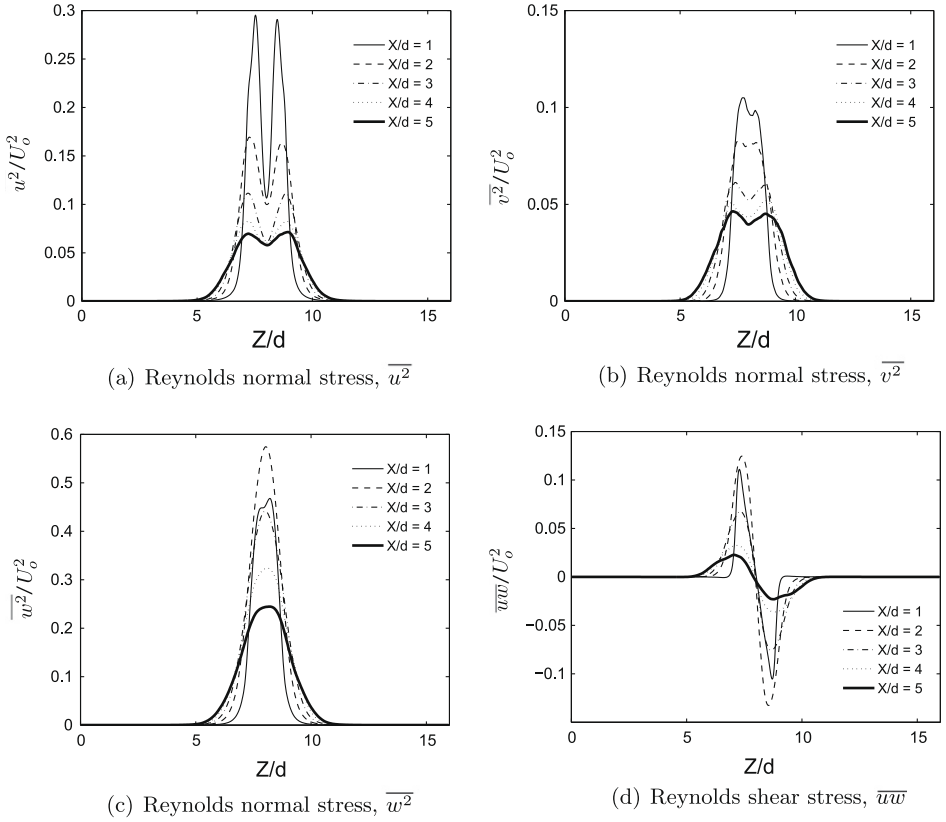

(a) Reynolds normal stress, $\overline{u^2}$ (b) Reynolds normal stress, $\overline{v^2}$

(c) Reynolds normal stress, $\overline{w^2}$ (d) Reynolds shear stress, $\overline{uw}$

Fig. 7. Reynolds stress profiles at fixed X/d positions (measured from the axis of the plate).

simple fact that $\partial U/\partial Z$ is the dominant mean shear rate, as convincingly demonstrated by Perrin et al. (2006). We therefore hypothesize that the turbulence produced locally in the shear layers remains *frozen* when the shear-layer rolls up to a vortex which in turn is transported towards the centre of the wake. The roll-up tends to convert streamwise momentum into cross-stream momentum.

While the streamwise and cross-stream Reynolds stress components comprise contributions from the shed vortex cells and real turbulence, it is obvious that spanwise fluctuations $\overline{v^2}$ consist of only turbulent fluctuations since the shedding is confined almost entirely in the (X,Z)-plane. However, the production term of spanwise velocity fluctuations is exactly zero in a planar mean flow and it is likely that $\overline{v^2}$ results from pressure-strain interactions which tend to drive the turbulence towards isotropy, i.e. to transfer turbulent kinetic energy also into the direction where no production takes place.

The variation of the mean fluctuating kinetic energy, $k = (\overline{u^2} + \overline{v^2} + \overline{w^2})/2$, is shown in Fig. 8a and the contribution of each normal stress component to the fluctuating kinetic energy along the wake centerline can be explored in Fig. 8b. The energy dissipation rate ε is associated with the small-scale velocity fluctuations which are damped by viscous action. The large-scale motions associated with the shed vortex cells do not contribute to ε, whereas the kinetic energy k comprises both real turbulence and the quasi-periodic cells. The bimodal pattern of ε clearly indicates that the maximum dissipation levels are offset from the wake centerline and occur in the shear layers. It is interesting to observe that the spatial variation of ε does not match the distribution of k. However, as argued above, the kinetic energy is not only produced locally but advected

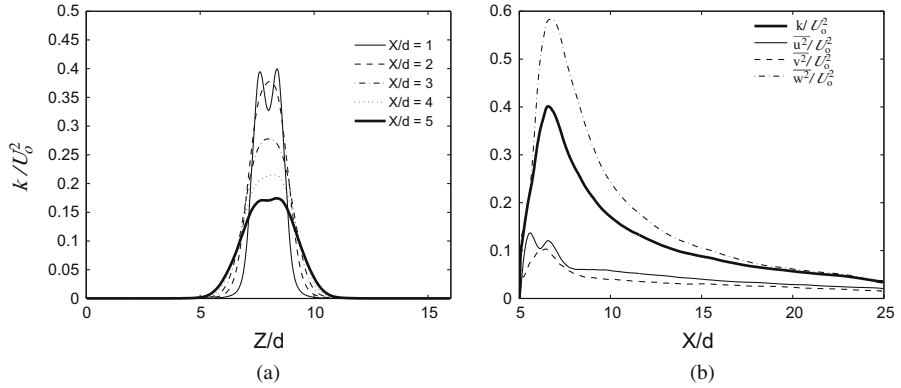

(a) (b)

Fig. 8. (a) Mean fluctuating kinetic energy $\left(k/U_o^2\right)$ profiles at fixed X/d positions (measured from the axis of the plate). (b) Mean fluctuating kinetic energy and Reynolds stress distribution along the wake centerline.

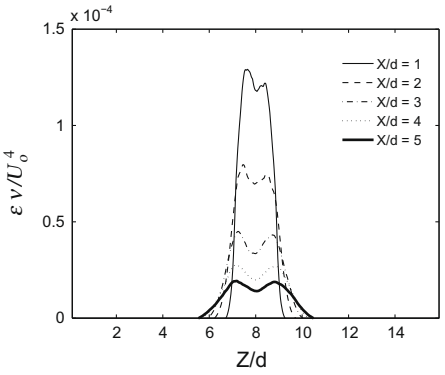

Fig. 9. Dissipation rate of fluctuating kinetic energy $\left(\varepsilon\nu/U_o^4\right)$ at fixed X/d positions (measured from the axis of the plate).

from the separated shear layers to the wake centerline. From the profiles in Fig. 9 it is observed that the energy dissipation rate exhibits a six-fold decay from $X/d = 1$ to $X/d = 5$, whereas the kinetic energy k is only reduced by a factor of about 2 (cf. Fig. 8a). This implies that the kinetic energy is only partially dissipated locally where it is produced.

Computations of vortex shedding behind bluff bodies by means of steady-state RANS solvers are deemed to fail since the embedded turbulence model is not designed for unsteadiness other than real turbulence. A turbulence model is therefore unable to account for the shed vortex cells. Unsteady RANS (i.e. URANS), however, may reproduce the quasi-periodic shedding as part of the resolved velocities and the turbulence model has to account only for real turbulence; see e.g. Ong et al. (2009) for a recent example. Leder (1991) furthermore argued that the anisotropy of the Reynolds stress field in the near-wake of a flat plate cannot be represented by a scalar quantity, i.e. a Boussinesq eddy viscosity. Schmitt (2007) more recently assessed the validity of eddy viscosity modeling and demonstrated that Boussinesq's hypothesis is valid only in a modest region of the wake behind a square cylinder.

4. Conclusions

The parallel-shedding characteristics of the wake behind a normal flat plate was well captured in the present DNS study. Both flow visualizations and spectral analysis together confirm this feature. The Strouhal number in the present turbulent flow case was found to be in excellent agreement with the previous studies on normal flat plates carried out at low Reynolds numbers (Saha, 2007; Najjar and Balachandar, 1998). In contrast the Strouhal number predicted by Najjar and Vanka (1995a) was found to be significantly lower. In addition, the predicted base pressure in Najjar and Vanka (1995a) was relatively higher than in the present case. The reason for this discrepancy was suggested to be due to the different Reynolds numbers used in the present study and in Najjar and Vanka (1995a). Another possible reason could be the coarse grid resolution adopted by Najjar and Vanka (1995a). The coupling between the base pressure and the vortex formation process was explored in the present study. It was observed that the reduction in base pressure causes a surge in the shedding frequency and hence produces a shorter recirculation bubble. A detailed analysis of the Reynolds-averaged statistical quantities was presented. It was noticed that the transverse velocity fluctuations were more energetic than the streamwise and spanwise velocity fluctuations and hence represented the major contribution to the fluctuating kinetic energy.

Acknowledgments

This work has received support from The Research Council of Norway (Programme for Supercomputing) through a grant of computing time. The first author was the recipient of a research fellowship offered by The Research Council of Norway.

References

Bearman, P.W., 1965. Investigation of the flow behind a two-dimensional model with a blunt trailing edge and fitted with splitter plates. J. Fluid Mech. 21, 241–255.
Bearman, P.W., 1967. The effect of base bleed on the flow behind a two-dimensional model with a blunt trailing edge. Aero. Q. 18, 207.
Bradshaw, P., Perot, J.B., 1993. A note on turbulent energy dissipation in the viscous wall region. Phys. Fluids A 5, 3305–3306.
Dennis, S.C.R., Wang Qiang, Coutanceau, M., Launay, J.L., 1993. Viscous flow normal to a flat plate at moderate Reynolds numbers. J. Fluid Mech. 248, 605–635.
Fage, A., Johansen, F.C., 1927. On the flow of air behind an inclined flat plate of infinite span. Brit. Aero. Res. Coun. Rep. Memo 1104, 81–106.
Jeong, J., Hussain, F., 1995. On the identification of a vortex. J. Fluid Mech. 285, 69–94.
Julien, S., Lasheras, J., Chomaz, J.-M., 2003. Three-dimensional instability and vorticity patterns in the wake of a flat plate. J. Fluid Mech. 479, 155–189.
Julien, S., Ortiz, S., Chomaz, J.-M., 2004. Secondary instability mechanisms in the wake of a flat plate. Eur. J. Mech. B/Fluids 23, 157–165.
Kiya, M., Matsumura, M., 1988. Incoherent turbulence structure in the near wake of a normal plate. J. Fluid Mech. 190, 343–356.
Leder, A., 1991. Dynamics of fluid mixing in separated flows. Phys. Fluids A 3, 1741–1748.
Manhart, M., 2004. A zonal grid algorithm for DNS of turbulent boundary layers. Comput. Fluids 33, 435–461.
Mazharoglu, Ç., Hacışevki, H., 1999. Coherent and incoherent flow structures behind a normal flat plate. Exp. Therm. Fluid Sci. 19, 160–167.
Mittal, R., Balachandar, S., 1995. Effect of three-dimensionality on the lift and drag of nominally two-dimensional cylinders. Phys. Fluids 7, 1841–1865.
Moser, R.D., Rogers, M.M., Ewing, D.W., 1998. Self-similarity of time-evolving plane wakes. J. Fluid Mech. 367, 255–289.
Najjar, F.M., Balachandar, S., 1998. Low-frequency unsteadiness in the wake of a normal flat plate. J. Fluid Mech. 370, 101–147.
Najjar, F.M., Vanka, S.P., 1995a. Effects of intrinsic three-dimensionality on the drag characteristics of a normal flat plate. Phys. Fluids 7, 2516–2518.
Najjar, F.M., Vanka, S.P., 1995b. Simulations of the unsteady separated flow past a normal flat plate. Int. J. Numer. Methods Fluids 21, 525–547.
Narasimhamurthy, V.D., Andersson, H.I., Pettersen, B., 2008. Cellular vortex shedding in the wake of a tapered plate. J. Fluid Mech. 617, 355–379.
Ong, M.C., Utnes, T., Holmedal, L.E., Myrhaug, D., Pettersen, B., 2009. Numerical simulation of flow around a smooth circular cylinder at very high Reynolds number. Mar. Struct. 22, 142–153.
Peller, N., Le Duc, A., Tremblay, F., Manhart, M., 2006. High-order stable interpolations for immersed boundary methods. Int. J. Numer. Methods Fluids 52, 1175–1193.
Perrin, R., Braza, M., Cid, E., Cazin, S., Moradei, F., Barthet, A., Sevrain, A., Hoarau, Y., 2006. Near-wake turbulence properties in the high Reynolds number incompressible flow around a circular cylinder measured by two- and three-component PIV. Flow Turb. Combust. 77, 185–204.
Persillon, H., Braza, M., 1998. Physical analysis of the transition to turbulence in the wake of a circular cylinder by three-dimensional Navier–Stokes simulation. J. Fluid Mech. 365, 23–88.
Saha, A.K., 2007. Far-wake characteristics of two-dimensional flow past a normal flat plate. Phys. Fluids 19, 128110.
Schmitt, F.G., 2007. About Boussinesq's turbulent viscosity hypothesis: historical remarks and a direct evaluation of its validity. C.R. Mecanique 335, 617–627.
Tamaddon-Jahromi, H.R., Townsend, P., Webster, M.F., 1994. Unsteady viscous flow past a flat plate orthogonal to the flow. Comput. Fluids 23, 433–446.
Thompson, M.C., Hourigan, K., Ryan, K., Sheard, G.J., 2006. Wake transition of two-dimensional cylinders and axisymmetric bluff bodies. J. Fluids Struct. 22, 793–806.
Wu, S.J., Miau, J.J., Hu, C.C., Chou, J.H., 2005. On low-frequency modulations and three-dimensionality in vortex shedding behind a normal plate. J. Fluid Mech. 526, 117–146.
Yao, Y.F., Thomas, T.G., Sandham, N.D., Williams, J.J.R., 2001. Direct numerical simulation of turbulent flow over a rectangular trailing edge. Theor. Comput. Fluid Dyn. 14, 337–358.